Determination of the correlation between soilborne pathogen inactivation and radio wave exposure

Sturm, G. S.J.; Linnenbank, S.; Bonnet, J.; van der Wurff, A.; Koppert, A.

DOI
10.1080/08327823.2025.2454719

Publication date
2025

Document Version
Final published version

Published in
Journal of Microwave Power and Electromagnetic Energy

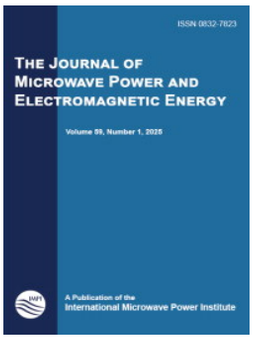

Taylor & Francis
Taylor & Francis Group

Journal of Microwave Power and Electromagnetic Energy

ISSN: (Print) (Online) Journal homepage: www.tandfonline.com/journals/tpee20

Determination of the correlation between soilborne pathogen inactivation and radio wave exposure

G. S. J. Sturm, S. Linnenbank, J. Bonnet, A. van der Wurff & A. Koppert

To cite this article: G. S. J. Sturm, S. Linnenbank, J. Bonnet, A. van der Wurff & A. Koppert (2025) Determination of the correlation between soilborne pathogen inactivation and radio wave exposure, Journal of Microwave Power and Electromagnetic Energy, 59:1, 46-74, DOI: 10.1080/08327823.2025.2454719

To link to this article: https://doi.org/10.1080/08327823.2025.2454719

JOURNAL OF MICROWAVE POWER AND ELECTROMAGNETIC ENERGY
2025, VOL. 59, NO. 1, 46–74
https://doi.org/10.1080/08327823.2025.2454719

Taylor & Francis
Taylor & Francis Group

RESEARCH ARTICLE

Determination of the correlation between soilborne pathogen inactivation and radio wave exposure

G. S. J. Sturm[a], S. Linnenbank[b], J. Bonnet[c], A. van der Wurff[d] and A. Koppert[b]

[a]Process & Energy department, Delft University of Technology, Delft, The Netherlands; [b]Koppert Machines B.V., Monster, The Netherlands; [c]Stichting Control in Food & Flowers, Delfgauw, The Netherlands; [d]Groen Agro Control, Delfgauw, The Netherlands

ABSTRACT

Radio wave treatment is considered as an alternative for steam treatment of soil in glasshouse horticulture for pathogen suppression. In principle, radio wave treatment can be selectively focused on localized infestations, as well as accommodate renewable energy sources. It may therefore help to significantly reduce fossil fuel consumption for soil treatment in greenhouse horticulture. A prototype treatment system has been developed prior to this study. Following this system's development, the next step is to develop optimum treatment strategies for its application. To this end, this study presents the development of an experimental method to perform quantified experimentation at laboratory scale on pathogen infested soil samples. The study is an interdisciplinary approach that merges respective contributions from microwave engineering, control engineering, and phytopathology. The design requirements for the experimental system are outlined. The design of the layout of the apparatus, computer simulations to optimize its geometry, and the design of power and temperature control are discussed. The study is finalized by reporting a demonstration of the experimental method.

ARTICLE HISTORY
Received 13 March 2024
Accepted 26 November 2024

KEYWORDS
Horticulture soil treatment; pathogen suppression; radio wave treatment; development of experimental methodology

Introduction

At present, steam treatment is employed for pathogen suppression in the context of open soil glasshouse horticulture. This method involves manually placing a large sheet over the soil bed, and injecting steam under this sheet over the course of hours (Dabbene et al. 2003; Bollen 1969). This method has several drawbacks. It is energy-intensive, having a fuel requirement of 4 to 6 cubic meters of natural gas per square meter of soil per treatment, or the equivalent energy demand in liquid fossil fuel. Moreover, in the context of the global energy transition, this particular usage of fossil fuel will become progressively more undesired, potentially even

CONTACT G. S. J. Sturm info@guidosturm.nl Process & Energy Department, Delft University of Technology, Leeghwaterstraat 39, 2628 CB, Delft, The Netherlands.

restricted. In addition, a shift to renewable electric sources has the inconvenience that a fluctuating source of renewable energy may not be able to keep the steam sheet inflated by a continuous steam supply, which may compromise the full treatment of the entire soil bed. Moreover, steam treatment is a labour-intensive process as the sheet is placed and removed manually, which cannot be automated.

In this context, an alternative technology named Agritron has been developed by Koppert Machines that employs radio wave heating of soil (Koppert Machines 2014; Figure 1). The photograph shows the prototype in operation. As it drives over soil, a magnetron in this vehicle generates a radio wave field in the 915 MHz ISM frequency band (International Telecommunication Union 2020) up to 100 kW of output power; horn antennas direct the field into the soil where the radio wave energy is converted into heat *via* dielectric heat generation. The inset figure (Figure 1) presents a thermogram (FLIR A655sc with 24.6 mm T197922 lens) that shows the path of elevated temperature that trails the vehicle. This treatment concept in principle avoids the shortcomings of steam treatment. It operates on electricity, which is compatible with renewable energy sources. Moreover, in principle, it can accommodate fluctuating renewable sources; adjusting the velocity of the vehicle during treatment enables it to maintain a consistent application of radio wave energy per unit treatment path length. As such, in addition to a potential solution for soil treatment, it might also be applicable as a demand response application. Such application facilitates stabilization of the electrical grid (Conchado and Linares 2012), for which electricity is traded on the intraday and imbalance markets (Agro Energy 2017; Welle 2016). Moreover, the treatment process is in principle amenable for automation, which would minimize the labour requirement.

The prototype treatment system is effective as it enables the suppression of undesired organisms in the soil. This leads to a new question: how to apply this technology? Analogous to a domestic microwave oven: the oven by itself does not make a meal, ingredients and recipes are also needed. The radio wave treatment system

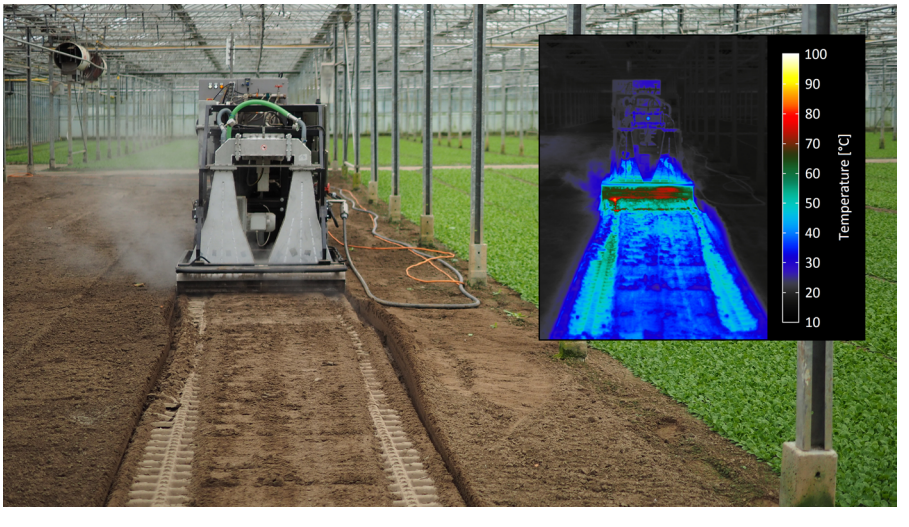

Figure 1. Agritron prototype in operation. The thermogram was recorded with a FLIR A655sc with a 24.6 mm T197922 lens.

for soil requires a protocol for effective operation. In other words, it also needs a recipe.

Study context

The direct context of this study is two prior studies (Sturm et al. 2023, 2024) in which we develop a numerical simulation of the radio wave treatment process to ultimately facilitate the development of treatment protocols. We explore the treatment process by means of this simulation, and we have found for example that variations in transport phenomena do not strongly affect treatment effectiveness, and it confirms the feasibility of the aforementioned adjustment of the vehicle velocity to compensate for electric power fluctuations.

One limiting factor that we encountered was the *lack of quantified experimental data* on the biological interactions. Such data would be essential for accurate simulation of the treatment process. Instead of a comprehensive biology description, only a placeholder model could be used in our prior studies based on a simple Arrhenius expression for pathogen inactivation.

To address this matter, we present in this present study the development of an experimental apparatus that allows us to quantifiably replicate the treatment conditions as they occur in soil during treatment with the Agritron treatment system. Figure 2 presents this purpose-built experimental apparatus, the TE_{10n} WR975 Experiment for Inactivation Kinetics (Tweik).

The Tweik-apparatus is a complementary development to the Agritron soil treatment system. The development of the apparatus is motivated by: 1) the desire for quantified correlations between radio wave exposure and biological responses; 2) a desire for experimentation at reduced cost and a more rapid rate of data generation as compared to field trials with the Agritron treatment system; and 3) the desire to perform experimentation on risk-bearing pathogens in a controlled laboratory environment so as to avoid contamination risks.

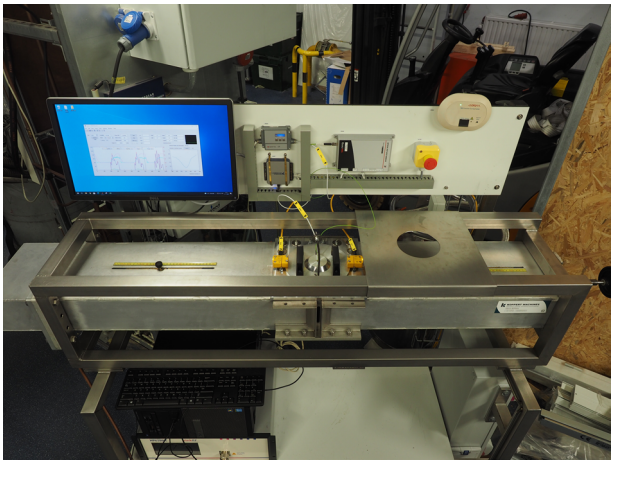

Figure 2. TE_{10n} WR975 experiment for inactivation kinetics (Tweik).

Background

By observing that there is a lack of experimental data for the specific application that we are developing, we do not mean to say that there is no data at all. On the contrary, much useful insight can be gained from prior research efforts. The first field of research that must be mentioned here is the topic of soil solarization. In the book on soil solarization edited by Katan and Devay (1991a), these authors mention in one of their own contributions (Katan and Devay 1991b) non-monotonic and interdependent biological interactions. They emphasize caution on 'disturbing the biological balance'. Their co-contributors Griffin and Baker (1991) and Chen et al. (1991) speak of 'the boomerang effect' in which excessive treatment results in an opportunity for pathogens to reinfest. Similar mechanisms are described by Roux-Michollet et al. (2010) in the context of steam treatment, where it is hypothesized that the slow dynamics of steam treatment permit time for bacteria to employ survival mechanisms against elevated temperatures. The result would be a subsequent opportunistic reinfestation. From these studies, it already follows that the biological processes that are at play must be expected to be considerably more complicated than mere monotonic inactivation behaviour of a single pathogen. Models for these processes would require for example: the inclusion of species behaviour – both pathogens and useful species; interactions between different species; and the availability of nutrients.

With respect to radio wave treatment in agriculture, much work has been done in past studies. The earliest studies data back to the 1950s to 1970s. Eglitis et al. (1956) and Eglitis and Johnson (1970) report on the suppression of Pythium in soil with a radio frequency field at 27 MHz. Seaman and Wallen (1967) report on the suppression of several seed-borne pathogens by means of a radio frequency fields of 59 and 94 MHz. Higher frequencies are explored for example by O'Bannon and Good (1971) and Barker et al. (1972) who apply the frequency of 2450 MHz to several pathogens. The frequency band of the radio wave field is clearly an important design parameter, so it is fitting that Nelson and Stetson (1974) report on a comparative study between the VHF and UHF bands at 39 MHz and 2450 MHz, respectively. They report on controlling an insect species (*S. oryzae*), and conclude that the lower frequency band of 39 MHz shows better potential for selective heating of insects. In the 1970s also the first applicator designs for treatment of a bed of soil appear as Menges and Wayland (1974) and Wayland et al. (1975) report on the development of such applicators that radiate at 2450 MHz onto soil for weed control. A study by Ferriss (1984) at this frequency mentions that microwave energy is effective, though only at small scale. Nevertheless a review by Nelson (1996) includes several works on soil treatment with electromagnetic fields, most involving a frequency of 2450 MHz and a few at 27 MHz or 40 MHz. Generally, the frequency of 2450 MHz appears to be in favour for experimental studies, presumably because of the availability of heating equipment that operates at this frequency. For example, other more recent studies that consider this frequency include: Rasing and Jansen (2007), who demonstrate the effectiveness of electromagnetic heating on potting soil and agricultural substrates; Brodie and co-workers (Brodie et al. 2012, 2015, 2020a, Khan et al. 2016), who investigate the utilization of microwave exposure for pest

control, weed management, and wheat preparation; Abbey et al. (2017), who report on the bioavailability of nutrients in response to microwave exposure; Miler and Kulus (2018), who report on mutation breeding of chrysanthemum under microwave exposure; and Mahdi et al. (2021), who report on the effect of microwave exposure on bacteria, fungi, and growth characteristics. The recurring selection of the 2450 MHz frequency in literature can be justified by the availability and familiarity of the associated equipment, in particular when the intended applications aims for a shallow treatment effect, or if the particular study is limited to a proof-of-concept scope. For applications like soil treatment that aim to treat larger volumes, the longer wavelength and treatment depth of a field at 915 MHz is more appropriate though. In addition, 915 MHz fields can be generated at higher power and better efficiency than 2450 MHz (personal communication with Radoiu 2011; Meredith 1998).

These considerations directed the selection of the 915 MHz band for the Agritron treatment system. Recently, more studies have appeared that consider this frequency range, such as Tkalec et al. (2009) (both 400 MHz and 900 MHz), Maynaud et al. (2019) (915 MHz), Hess et al. (2018, 2019) (915 MHz), and Brodie et al. (2020b) (both 2450 MHz and 922 MHz).

In order to replicate the conditions in soil during treatment with the Agritron system, we could not rely on of-the-shelf experimental microwave devices. The frequency band that they operate in does not match the one that is employed by this treatment system. This by itself could motivate the development of an experimental apparatus that enables experimentation at 915 MHz. However, there are additional drawbacks to of-the-shelf experimental laboratory systems. Typical of-the-shelf laboratory microwave heating devices (e.g. CEM Corporation 2020; Anton Paar GmbH 2021; Milestone Srl 2021) do not provide any particular control over the spatial distribution of radio wave energy (Sturm et al. 2012), nor allow recording of the total transmission of energy (Sturm et al. 2013a). Furthermore, accurate temperature measurement in these devices is a long-standing topic of debate (Kappe 2013). Note that this is no objection if the particular experimental device is used for its intended purpose, i.e. to provide convenient lab-scale heating, it only becomes an issue once precision is required in the application of radio frequency energy.

Study objectives and outline

The primary objective of this study is the creation of an experimental apparatus to replicate the conditions in soil during treatment with the Agritron radio wave treatment system, in particular the conditions during radio wave exposure. In addition, we demonstrate the resulting apparatus, the TE_{10n} WR975 Experiment for Inactivation Kinetics (Tweik) apparatus, in order to advance the development of experimental protocols to explore the correlation between radio wave exposure and biological response in soil. As mentioned before, the main advantages that we see for this laboratory-scale experimental system are: better-quantified correlation; reduced expense, and larger volume of data generation as compared to field trials with the Agritron system; and a controlled environment to safely experiment with risk-bearing soil-borne pathogens.

We intend to report our findings such that the design and development of our experimental system can be replicated and elaborated upon in a multi-disciplinary setting. This article therefore discusses first the requirements for the apparatus in detail, which is followed by a description of the physical aspects of the apparatus design. These aspects are: the sample holder; the design of the radio wave circuit, the selection of the solid-state radio wave generator, numerical simulation to establish a tuning recommendation for the radio wave circuit, and a discussion on extended experimentation following the radio wave exposure. Subsequent to the physical design of the apparatus, the control system for radio wave application is discussed. We explain our preference for a more advanced predictive control arrangement, instead of a more typical arrangement of PID-control with a feedforward loop. Finally, we demonstrate the experimental methodology for which the apparatus is developed. We first demonstrate its ability to replicate the temperature transients that occur during radio wave exposure by the Agritron treatment system. Subsequently, we demonstrate experimental procedures to assess the sensitivity of a nematodes species (*S. feltiae*) to the exposure profile of the Agritron treatment system as replicated by the Tweik-apparatus.

Requirements for the experimental apparatus

The main purpose of the experimental apparatus is to replicate the conditions in soil during treatment with the Agritron system to establish quantified correlations between radio wave exposure and biological effects in the exposed soil samples. To establish a description of what the conditions in the soil during treatment are, a temperature transient (Figure 3, left) is measured in a bed of soil during a field trial with the Agritron system. The measurement was performed with a fibreoptic sensor, i.e. a Rugged Monitoring Lsens-U sensor, which was positioned at a depth of 20 mm centered under one of the horn antennas of the prototype. This particular type of sensor is used because it tolerates the high-intensity radio wave field and because it is sufficiently mechanically robust to endure the test conditions.

In addition to the temperature transient, a transient for the rate-of-change of temperature per unit time is calculated (Figure 3, right). Temperature rate-of-change is closely related to the heat generation process. By approximation the two are proportional, provided that the dynamics of heat transfer are ignored. The rate-of-change graph therefore describes the progression of heat generation; it suggests that the application of radio wave energy follows a triangular profile. Specifically, the trend is that the temperature rate-of-change curve initially rises at an approximately constant rate up to a maximum. After reaching this maximum, the temperature rate-of-change initially drops at about the same rate as it was rising. Eventually, the curve deviates from a purely triangular profile and forms a decaying tail due to the dynamics of heat transfer. In total, heating lasts for approximately 120 s.

The operating frequency of the Agritron system is in the 915 MHz ISM frequency band, and therefore, our experimental system needs to operate at the same frequency. The exposure needs to be defined primarily in terms of temperature so as to enable correlation to kinetic studies on pathogen inactivation (Peleg et al. 2012; Fujikawa and Itoh 1998; Pullman et al. 1981). In addition, another relevant measure would be the amount of radio wave energy expended per unit mass of soil, as this is an important

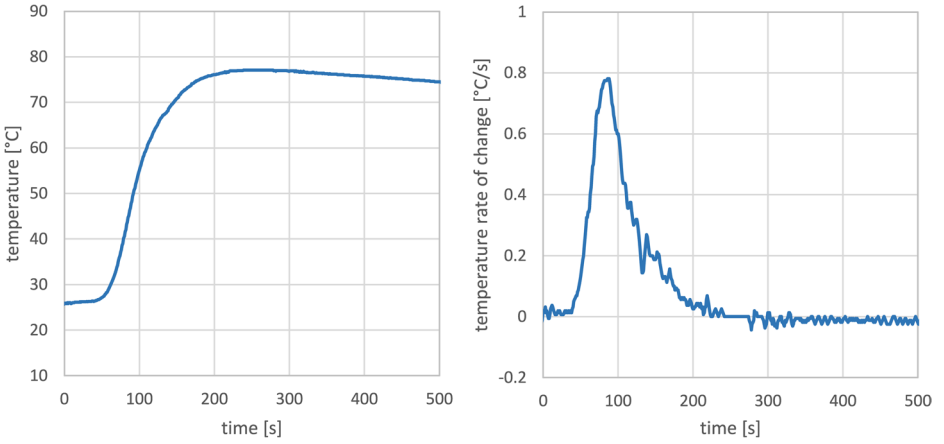

Figure 3. Temperature transient (left) was acquired during a field trial; from this transient a temperature rate-of-change graph was calculated (right). The data were recorded with a Rugged Monitoring Lsens-U fiber optic sensor, which was positioned at a depth of 20 mm in the soil under the path of the centerline of one of the horn antennas.

parameter in determining the viability of an energy-intensive process like radio wave treatment. A final requirement is the need to heat a sufficiently large volume of soil in order to facilitate biological tests. We ultimately performed our demonstration on nematodes, and we selected the Oostenbrink elutriator for final sample analysis, primarily because of its availability. Selecting another analysis method would not have allowed for a much smaller minimum volume though, since all suitable methods have sample sizes of the same 100–1000 ml order of magnitude as reported by OEPP/EPPO (2013). A minimum sample volume requirement was decided upon at the lower end of this range at 100 ml (personal communication with Keidel 2019).

Physical apparatus design

The aspects of the apparatus design that are presented in this section are the design of the radio wave circuit, the design of the sample holder, the selection of the radio wave generator, and the tuning recommendation for the tuning elements of the radio wave circuit. The dimensioning of the apparatus is not performed for each aspect separately but instead, an integrated design is developed *via* numerical simulation.

Sample holder

The minimum volume requirement of 100 ml poses a challenge. Due to the spatial size of standing wave patterns in a resonant cavity, the volume in which the heat generation is distributed uniformly will always be restricted to some degree. This depends on the geometry and the dielectric permittivity of the objects that interact with the standing wave field. Nevertheless, uniformity is an important criterion for out experimental system. Specifically, if the heating rate were to be unevenly distributed, then the temperature distribution would also be distributed unevenly, and this distribution effect would obscure the correlation between the temperature of

the soil sample and the inactivation of the pathogen population. For example, a situation may occur in which the main temperature development occurs only locally in the vicinity of a temperature sensor. In that case, colder zones will remain undetected, in which the pathogen population in the test sample is inadequately exposed to an elevated temperature. In such a case, the correlation between radio wave exposure and temperature versus the pathogen effect appears unfavourable, since more pathogens remain than would be expected for the seemingly well-exposed sample.

To illustrate the physical limitation on the uniformity of the radio wave exposure of a sample for our present design case, we apply the analysis in Sturm et al. (2010) on a soil sample with a real relative permittivity value of 20 and a uniformity requirement of 70%. From that analysis, it follows that we would have maximally a feasible sample volume of only 42 ml. This conflicts with the minimum volume requirement of 100 ml.

This is an unfortunate limitation of a stationary oscillating resonant field. It is physically impossible to uniformly distribute instantaneous heat generation from a 915 MHz resonant field over a volume of 100 ml. For the design of the Tweik-apparatus, therefore, we opted for a trade-off by placing the soil sample on a rotating platform. This may cause the heat generation in a specific location in the soil sample to cycle with the rotation, but on a time-averaged basis, heat generation and temperature are made uniform in the direction tangential to the axis of rotation. This helps to reach the best degree of uniformity that is feasible under the 100 ml requirement.

More advanced alternative design concepts may be considered for future developments that manipulate the spatial distribution of the standing wave field around a sample holder. Active mode convertors may cycle through a series of modal patterns that are excited in the cavity such that the time-average heating rate distribution is uniformly distributed in the sample. For example, an arrangement could be conceived in which the high-intensity electric field component is made to rotate around the sample, instead of rotating the sample with respect to the field as is the case in our apparatus. Such arrangement would demand a much higher degree of complexity on the radio frequency system, though. Nevertheless, it may potentially enable a much higher rate of relative rotation between sample and field, and could in principle allow for a higher degree of flexibility of temperature sensor placement. For our present design case, however, the limitations of a rotating platform are no impediment. Therefore we opted for this simpler arrangement.

The sample holder (Figure 4) is axially symmetric to accommodate the redistribution of radio wave energy through rotation when it is placed on the rotating platform inside the resonant cavity. In addition, the sample volume contained by the sample holder has a rounded top and bottom to improve the uniformity of the radio wave field in the sample volume. The volume holds 104.5 ml of soil, which satisfies the minimum volume requirement. The rotation speed is set to 25 rotations per minute.

These sample holders are machined from polyethylene because of its low dielectric loss factor. Specifically the complex relative permittivity as reported by Meredith (1998) is 2.25–0.0005i, the latter imaginary term being the loss factor, which is indeed rather low. Because it has this low value, only a very small amount of parasitic electromagnetic dissipation is expected to occur in the wall of the sample holder, so that this does not influence the experiment. Essentially all heat generation due to radio wave dissipation occurs in the soil sample itself.

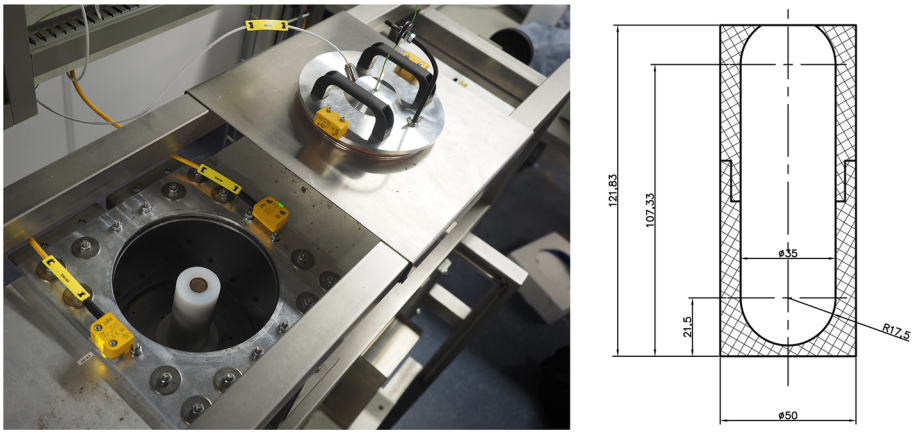

Figure 4. Left: position of sample holder in TWEIK-apparatus, right: dimensions of sample holder.

An important note has to be made here regarding the grade of polyethylene that is used to machine the sample holders form. Various grades in terms of molecular weight are available, but also varieties that contain additives to improve the mechanical properties of the material. We found an important difference between two varieties of polyethylene that are distinguished by their colour. One has the natural white colour, while the other is black due to additives in the material. Dielectric properties measurements lead us to recommend against the use of the black variety for this application, because the additives significantly increase the loss factor.

This dielectric properties measurement has been performed with an Agilent 85070E Performance Probe in combination with an Agilent E5071C network analyser and an Agilent N4691B ECal module. Both varieties of polyethylene have been assessed over the relevant temperature range of 20 °C to 85 °C. The precision of the measurement was limited by the contact that could be maintained between the probe and the sample under test. Nevertheless, it was found that the white variety would have a real relative permittivity value of 1.9 to 2.05, and a dielectric loss factor that is too low to be measured reliably, which corresponds loosely with the literature value (Meredith, 1998). The black variety of polyethylene, however, presented a real relative permittivity value of 2.5–3.04 and a loss factor of ~0.15. This suggests at least qualitatively that – despite the measurement inaccuracy – the additives in the black variety have significantly increased the loss factor to such a degree that this material cannot be considered a low loss material. Hence, parasitic absorption of radio wave energy inside the wall of the sample holder is to be expected, which would make this material an unsuitable option to manufacture sample holders from.

Circuit design

The radio wave circuit of the experimental apparatus is based on a standard sized rectangular waveguide, i.e. the WR975 standard waveguide size. For a recent overview of these standards, see for example Nickel (2022). Using standard waveguide elements allows utilization of the wide variety of available of-the-shelf microwave or radio

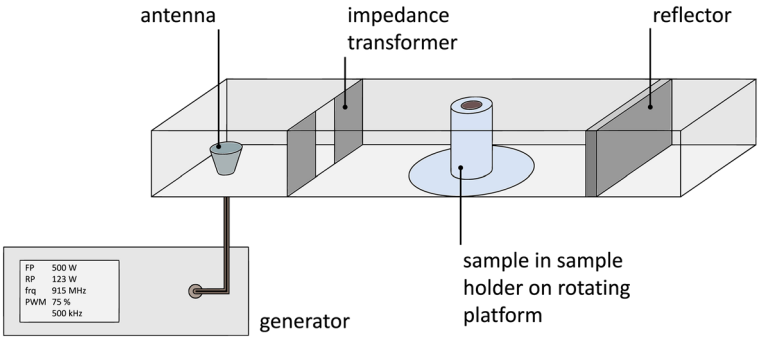

Figure 5. Schematic of the layout of the setup.

wave circuit elements, while permitting flexibility with respect to the exact design configuration. Moreover, the radio wave field forms a single-moded predicable TE_{10n} standing wave pattern (Pozar 2005) inside this waveguide. Appropriate tuning elements incorporated in a cavity design of this type allow for manipulation of the standing wave field to optimize uniformity and power transmission as will be explained below.

The schematic in Figure 5 shows the configuration of the radio wave circuit. From left to right, there is the antenna that couples the radio wave field that is generated by the generator into the cavity, then there are subsequently, the impedance transformer, the sample on its rotating platform, and the reflector. The purpose of the impedance transformer is to minimize reflection losses from the cavity back towards the generator. A global description of its working principle is as follows. Radio wave fields generally scatter – or reflect – off the objects that they interact with. As the field is transmitted into the cavity, one can expect that a large portion of its energy to be reflected back towards the generator if no particular measures are taken to avoid this. This is known as reflection loss. The purpose of the impedance transformer is to create additional reflections that interfere destructively with the reflections that are already present, thereby minimizing the resulting reverse wave, which minimizes the reflection loss. Next in the resonant cavity is the section in which the sample is placed. As explained, the sample is contained in a sample holder that is placed on a rotating platform. Above it, there is a quickly removable lid with a through hole for a fibreoptic temperature sensor. This is the primary temperature sensor to record the sample temperature. It is a Rugged Monitoring Lsens-T sensor, positioned inside the sample with a borosilicate sensor holder tube. In addition, a secondary temperature sensor is mounted in the lid. This is an infrared temperature sensor (Optris CT) that records the temperature of the top of the soil sample. The final element of the resonant cavity is the variable reflector that enables positioning of the radio wave field.

Radio wave generator

Up to recent years, all commercially available generators were based on magnetron technology. That type of generator in the 915 MHz band is less suitable for the purposes intended here, as it is large, expensive, and outputs too much power.

However, in recent times, generators have emerged that are based on solid state technology, which provides a more suitable radio frequency source (Werner 2020; Aguilar Garib 2022; Brown 2022). This has opened up possibilities for laboratory scale experimentation, in particular at this frequency. A PinkRF MPG1000L solid state generator is installed in the Tweik-apparatus. This generator provides radio wave power at a variable frequency in a band from 902 to 928 MHz at a power that is continuously variable between 0 and 1 kW. A Siglent SVA1015X spectrum analyser/VNA is used to confirm that the radio wave field is generated in a < 1 MHz band around the set frequency. An additional advantage of solid state generators is that they enable precise measurement and control of the forward and reflected radio wave power, which thus allows for improved monitoring of the overall energy balance. A final useful feature that this particular generator has, is that it allows for pulse width modulation so that the effect of a ripple in the power output on the soil treatment process can be mimicked if so desired for evaluation.

Design dimensioning through numeric simulation

To optimize the design of the experimental system, the radio wave field and heat generation are simulated in Comsol Multiphysics 5.5 (COMSOL AB 2019; Figure 6). The simulation is used to determine several design variables. The first set of variables is the exact geometry of the sample holder as described above. Furthermore,

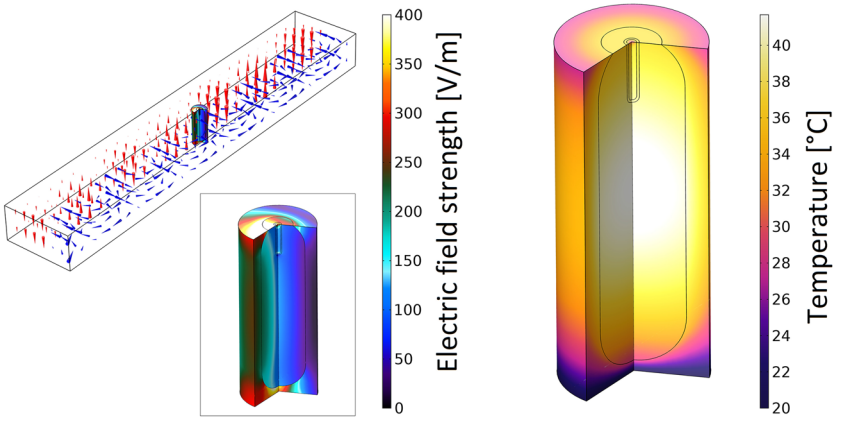

Figure 6. Simulation of electromagnetic field (left) and heat transfer (right) in sample holder. The vector fields in the left figure show the electric (red) and magnetic (blue) field in the waveguide cavity to illustrate the morphology of radio wave field in the TE_{10n} mode. This mode is the fundamental one, all other modes are suppressed for an appropriately chosen waveguide size and frequency. The designation TE_{10n} means that the electric field vector is perpendicular to the length of the waveguide, and that the standing wave field has one field maximum over the width of the waveguide, zero maxima over the height making it invariant in that direction, and an arbitrary number *n* along the length of the waveguide. Note that this rendering has the view on electric and magnetic components split over the two halves of the waveguide. It is displayed in this manner for clarity so that the field morphologies can be apprised better, while in reality both field components stretch over the entire cavity volume.

simulation is used to determine the optimum reflector position for the best uniformity of heat generation in the soil sample. Finally, simulation is used to find the position for the fibreoptic temperature sensor in the sample that best matches the average temperature of the sample during the heating cycle.

The equation that is used to simulate the radio wave field is the time-harmonic Helmholtz wave equation for the electric field vector **E**,

$$\nabla \times \frac{1}{\mu_0}\left(\nabla \times \mathbf{E}\right) - k_0^2\left(\varepsilon_r\right)\mathbf{E} = 0 \tag{1}$$

The coupled magnetic field can be derived from the electric field if needed. The media under consideration have no particular magnetic properties, so the magnetic permittivity of vacuum (μ_0 = $4\pi \cdot 10^{-7}$ H/m) is applied throughout these simulations. The symbol k_0 is the wave number of free space, $k_0 = \omega/c_0$, where ω is the angular frequency ($2\pi \cdot 915$ MHz = $5.75 \cdot 10^9$ rad/s). The medium parameter that affects the radio wave field is the relative dielectric permittivity. Since a time-harmonic representation is used for the electromagnetic interactions, the medium properties are expressed as a complex valued parameter,

$$\varepsilon_r = \varepsilon' - i\varepsilon'' \tag{2}$$

The real valued part of the permittivity (ε') accounts for the amount of electrical energy stored per unit volume of the medium at a particular field strength, while the imaginary part (ε'') represents the dissipation of electrical energy into heat. Heat generation is calculated through Eq. (3),

$$Q_{RF} = \frac{1}{2}\omega\varepsilon_0\varepsilon''\mathbf{E}\cdot\mathbf{E}^* \tag{3}$$

The symbol ε_0 is the vacuum permittivity (~$8.85419 \cdot 10^{-12}$ F/m). Heat transfer is implemented through the equation for heat conduction,

$$\rho C_p \partial_t T + \nabla \cdot \left(-\kappa \nabla T\right) = Q_{RF} \tag{4}$$

A redistribution function is implemented on the distribution of heat generation to account for the rotation of the sample. The thermophysical parameters are obtained from Mills (1999) and are 2 W/mK for the thermal conductivity of soil (κ), 1800 kg/m^3 for the density of soil (ρ), and 2280 J/kgK for the heat capacity (C_p). The properties for borosilicate glass of the sensor holder, polyethylene for the sample holder, and stagnant air in the sensor holders are implemented *via* the materials library of Comsol Multiphysics. A heat transfer coefficient of 20 W/m^{2}K is applied to the outside of the sample holder as an earlier study revealed this to be a good rule of thumb value for objects that are heated in metallic applicator cavities of comparable dimensions (Sturm et al. 2013b).

Four cases are simulated to decide the aforementioned design parameters. The cases are differentiated by the dielectric properties of the soil samples. These

properties are determined both through personal communication with J.F. Rochas (2021) on prior measurements, as well as through a new series of measurements on soil samples. The new measurements are performed with the same instrumentation as mentioned above (85070E Performance Probe, E5071C network analyser, N4691B ECal module, all manufactured by Agilent). The dielectric medium properties are measured of several soil samples that have been provided by horticulture growers. The resulting relative dielectric permittivity values are $2.03 - 0.1827i$, $8 - 1.6i$, $12.9 - 2.86i$, and $19.6 - 4.57i$.

The outcome of the simulation study is outlined as follows,

- The optimum position of a fibre optic temperature sensor is 102 mm above the cavity floor.
- The sample holder geometry is as described in Figure 4.
- Finally, an optimum tuning recommendation for the reflector is developed.

The recommendation for optimum tuning is applied as follows. First the sample to which the radio wave circuit is tuned is placed in the cavity without impedance transformer. The reflector is swept over its stroke while the generator is sending a low power signal to record the reflected power fraction. Subsequently the reflector position is determined that minimizes the reflected power fraction. For optimum uniformity of heating the reflector position is shifted a distance of 1/8 times the phase wavelength away from the sample. This amounts to a distance of 55 mm. The impedance transformer is then placed back into the cavity, and tuned to minimize the reflected power fraction; a reflected power fraction of around 10% is achieved for typical soil samples.

The four simulation cases each yield a set of temperature transients that aim for a final temperature of 70 °C, and are reached with a triangular profile, as described in the section on requirements (Figure 7). These simulations apply the tuning recommendation as described above. The graphs show the sensor temperature, as well as the average sample temperature with an indication of the average absolute deviation of the temperature field in the sample with respect to the average temperature. It can be observed that with higher dielectric permittivity the spread in sample temperature increases. Over the four simulated cases, the sensor temperature falls both above and below the average temperature, so a systematic error in one particular direction is avoided. In addition, after 120 s of heating, the sensor temperature approximates the average temperature, so for the overall treatment the sensor reading is an adequate quantification of the treatment intensity.

Conductive heat transfer out of the sample and sample holder will always concur with a temperature gradient inside the soil sample. Moreover, the variability of the electromagnetic medium properties of soil samples forms a disturbance on the heating process. Perfect temperature uniformity is therefore physically infeasible. Consequently, the geometry design and tuning recommendation form a compromise that allow for adequate agreement between the sensor reading and the average temperature of the soil sample. Better agreement between sensor temperature and sample temperature, and better sample temperature uniformity may in principle be feasible, but only if the requirement for a minimum sample volume of 100 ml is relaxed.

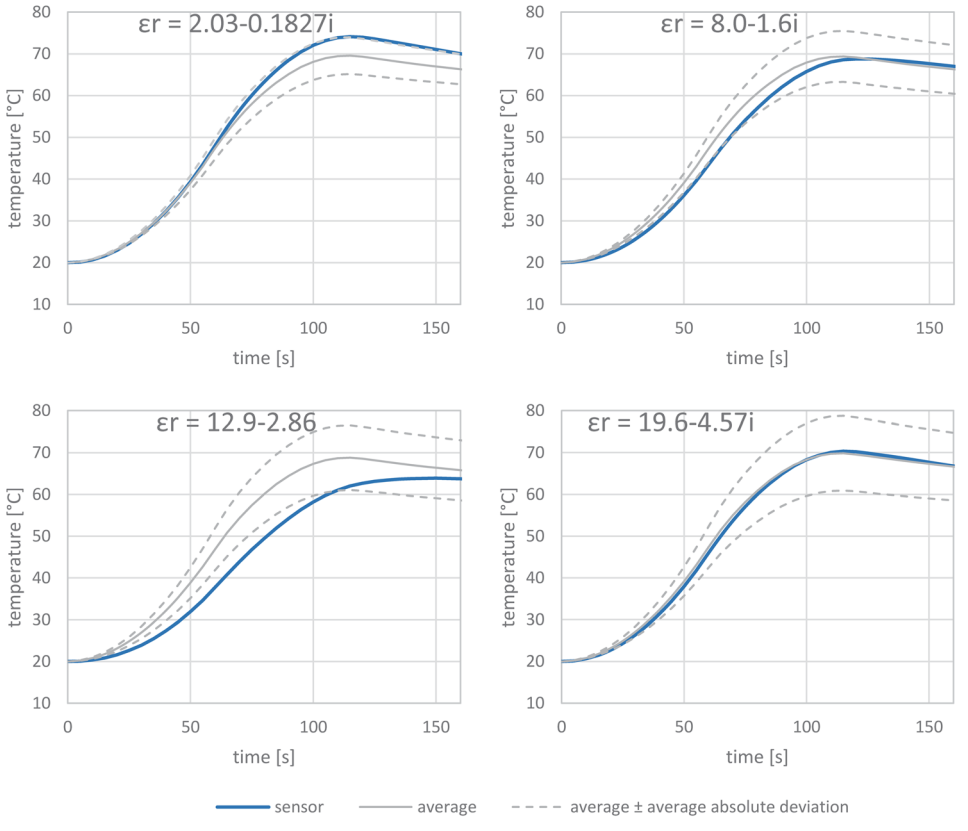

Figure 7. Simulated temperature transients of four soil samples heated in the TWEIK-apparatus. The respective dielectric medium properties of the four samples are included in the graph; the thermophysical parameters of the samples in the respective simulations are identical and are as presented in the main body text. In these simulations, the reflector position is tuned in accordance with the tuning recommendation that is described in the main body of the text, and the sensor is positioned in the position of the final design.

Post-exposure effects

For the minutes to hours after radio wave exposure, the conditions of the radio wave treatment as performed in a horticulture operation cannot be uniquely defined. For example, during the treatment process with the Agritron, the top layer of soil loses heat to the surrounding air, causing it to cool down relatively quickly. In contrast, deeper soil layers initially are shielded by the higher layers, so they do not heat up as much as the higher layers. After radio wave exposure, however, they receive heat from the hotter higher layers. Consequently, in deeper soil layers, temperatures first rises quickly due to radio wave exposure, but not as much as higher layers; then they experience a gradual temperature increase due to heat transfer from higher layers, before finally slowly cooling back to ambient temperature. In conclusion different vertical positions in soil experience qualitatively different long term temperature transients. It must be noted though, that our past studies (Sturm et al. 2023, 2024) suggest that the post-exposure long term temperature transients have marginal influence on the effectiveness of the treatment.

The Tweik-apparatus is not well-suited to replicate these long term temperature dynamics. Not least because it holds a relatively small soil volume in a metallic cavity, which creates an environment that draws out heat from the sample much more readily than a soil bed in a glasshouse environment. In case experimental evaluation post-exposure over longer time periods is desired, we recommend augmenting the experimental system with a programmable thermostatic bath. As such, soil samples in their holders can be relocated directly after a radio wave heating cycle into this bath so that a desired long term temperature profile can be applied to the soil sample. This would enable ample flexibility with respect to the desired long term temperature transients.

Temperature control system design

The requirements for the temperature control system are to apply radio wave power in a triangular profile to reach a pre-determined temperature in the sample in a time interval of 120 s. It may appear to be a simple single-input single-output control problem, though there are complicating factors.

A few issues relate to the manner in which the sensor is positioned in a glass sensor holder. This sensor holder is a glass tube, 3.5 mm inner diameter, in which a round bottom is made. It sticks into the soil sample at a fixed position, and it rotates with the soil sample, but the sensor does not. The sensor is grabbed by a rubber pad above the sensor holder, which presses it downward under a slight force, so that the tip of the sensor contacts the bottom of the sensor holder. Consequently, the sensor is in permanent contact with the bottom of the sensor holder, while the sensor holder loosely fits around it, so that this holder can freely rotate around the sensor. In this manner the position of the sensor is fixed, and the rotation of the soil sample is accommodated.

Nevertheless, the contact of the sensor with the wall of the sensor holder is not particularly intimate. In addition, the contact of the sensor varies as the sensor holder rotates around it. This causes a degree of sensor noise, as well as a delayed measurement response.

Another matter that needs to be accommodated is the zero power constraint of the radio wave generator, i.e. power cannot be negative.

Two control techniques have been applied to this control problem: PID control with PD feedforward, and model predictive control. The former might be considered an acceptable first design attempt, though nevertheless we would not recommend it. The latter technique is a more advanced method that ultimately proved more successful. Both are discussed here as both could be considered adequate, though the latter more so than the other one.

PID control

The first approach that is attempted for the control system design is a classical PID feedback controller (described in many textbooks, including tuning methods, e.g. Ogata 2002, or Franklin et al. 1994), with PD feedforward. Please refer to the schematic of the control system in Figure 8. The feedback loop first calculates the

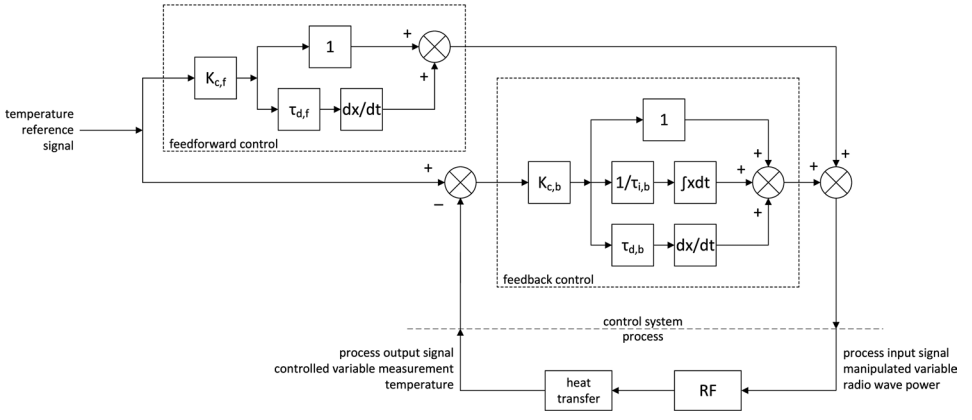

Figure 8. Schematic of PID control.

difference of the signal that provides the desired temperature reference signal with the measured actual temperature. This difference is then subjected to a proportional gain, an integration operation, and a differentiation operation. The results of the respective operations are summed, and the resulting sum is in many control problems directly used as the manipulated input variable for the process that is being controlled. Three tuning factors – $K_{c,b}$, $\tau_{i,b}$ and $\tau_{d,b}$ – are used to multiply the signals with to tune the controller for a particular performance.

The three different actions of this type of controller have different purposes, the proportional action has a stabilizing effect and makes the controller act quickly; the integral action regulates the error between measurement and reference signal to zero over time, but may cause controller instability; and the differentiating action corrects dynamic error variations and also dampens instabilities.

In practice, a PID controller is often tuned heuristically or by applying a tuning method like the Ziegler-Nichols tuning method. The aforementioned reference materials include descriptions of common tuning methods. For this particular application though, a stable and sufficiently performant closed loop PID feedback controller could not be so readily achieved. The issues with the sensor mounting are the cause of this. The time delay in the response tends to cause instability by repeated overcorrection, and the continually varying sensor contact hampers the tuning process. Therefore a more involved method was applied. First *via* non-parametric system identification (Ljung 1999) a frequency response of the system was obtained, which was then used to fit the open loop Nyquist curve to a performance characteristic that was defined by M-circles. Refer to reference material for a detailed description, for example Ogata (2002) provides a good description of these mathematical tuning aides. In the tuning procedure that we applied, the maximum closed loop overshoot was traded with bandwidth until a satisfactory response was obtained.

Finally, integrator anti-windup was applied to the integrating action of the feedback controller. Instances may occur in which the zero power constraint is exceeded. In such cases, the anti-windup resets the integrator so that the controller output signal remains within the actuation range of the generator.

In addition to a feedback controller, a feedforward PD-loop is was also included as is shown in the schematic. This control loop receives the reference signal for temperature and uses this to predict the radio wave power signal for which the temperature response approximates the desired reference trajectory. In this arrangement, the feedforward and feedback loops are complementary. The former enables a quick response to a change in reference signal, while the latter regulates the difference between temperature reference and measurement to zero. An approximate first order response was derived from the step response of the system, which was used to define the control parameters: $K_{c,f}$ is the inverse of the approximate first order steady state gain, and $\tau_{d,f}$ equals the time constant of the first order approximation.

The temperature reference signal consists of two parabolic profiles that form an s-shaped curve that reaches the desired final temperature and remains constant once it has been reached. Consequently, the time derivative of the reference consists of two linear profiles, which together from a triangle, similar to the profile of the right graph of Figure 3.

The overall performance of the control system as shown in the schematic (Figure 8) was marginally adequate. It suffered from a high amplification of sensor noise in the radio wave power, and also from a temperature overshoot that had to decay away through heat transfer. The latter was caused by the lack of control authority of the control system once temperature is too high, because it can only apply heat, while it cannot actively cool.

Overall, the controller as described in this section has a performance that may be considered adequate, though we would not recommend this PID arrangement with PD feedforward because of these issues.

Model predictive control

An alternative approach that is considered here, and which was eventually selected, is the Model Predictive Control (MPC) technique. The technique in general can also be referred to a Predictive Control or Model-Based Predictive Control. The operating principle can be implemented in various manners and a large number of MPC-methods exist. The first pioneering methods, Model Predictive Heuristic Control (Richalet et al. 1978) and Dynamic Matrix Control (Cutler and Ramaker 1980) emerged in the late 1970s and early 1980s. Over the years, there have been re-formulations of the technique and unifications, such as Generalized Predictive Control (Clarke et al. 1987), Unified Predictive Control (Soeterboek 1990) and the Standard Predictive Control Problem (Van den Boom and de Vries 1999).

The operation of a predictive controller versus a non-predictive controller can be illustrated by the task of keeping a driving car on the road. A non-predictive controller can only look out the side window at the edge of the road, and use that information to steer the car; information about the road ahead is not available. In contrast, a predictive controller does have the ability to anticipate future events.

Generally, the operating principle of predictive controllers is as follows. At each time step the controller calculates the optimum input signal(s) that will cause the output signal(s) to track (a) desired reference signal(s). The calculation is performed

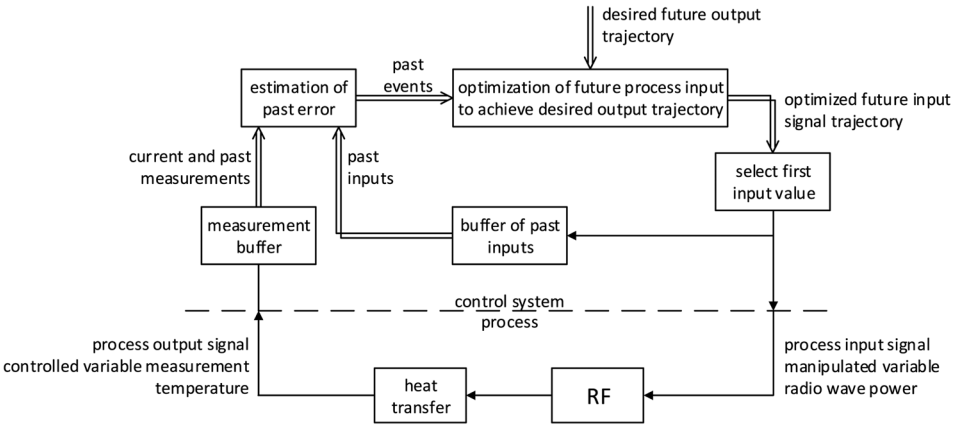

Figure 9. Schematic of MPC control.

over a pre-determined finite time-period. After each calculation, only the optimized input signals of the first future time step are applied to the system that is to be controlled. Subsequently, the system is sampled again, and the next output signal measurements are recorded and made available to the controller. After this, the optimum trajectory calculation is repeated in a cycle that repeats at each time step. This operation is illustrated by the schematic in Figure 9. The prediction horizon over which the calculation is performed recedes with each time step (receding horizon principle); the optimization therefore does not end at a particular instance in time, but it recurs at each time step for as long as the controller remains active. Due to this particular operating principle, predictive controllers have the ability to anticipate and account for future events, such as system responses that occur only after a time delay, or constraints that the input or output signals may encounter over their respective trajectories. Predictive controllers are therefore better able to handle such events than controllers without predictive features, such as PID controllers.

A more in-depth description of the implementation of the predictive controller that is used in this study is provided in Appendix A. The exact method is fairly basic but sufficient for the problem at hand. More advanced designs could be considered (e.g. as presented in the textbook by Camacho and Bordons (1995), but for the purpose of the control problem in this study, there would be no need for those. The reference signal that is supplied to the controller is the same as described in Section 'PID control'.

The controller is implemented *via* a real-time MATLAB (The Mathworks 2019) application. Communication to the generator is established *via* RS-232, and the analogue temperature signals are captured through a National Instruments USB-6001 I/O device.

Demonstration of experimental system

The experimental methodology is demonstrated through two sets of experiments. First the replication of a triangular heating profile is verified, and second a series of radio wave exposure experiments is performed on the nematode species *S. feltiae*.

For the first set of experiments, four soil samples (obtained from the verge garden in front of the Process and Energy department) were prepared to represent the variety of the horticulture samples that the setup is intended to operate with. Three of these are packed at moderate density into the sample holder with each prepared at a different soil humidity of 10, 17.5, resp. 25 m%. The fourth sample is at 25 m% humidity but is poured into the sample holder in a loose packing. Each sample is placed into the Tweik-apparatus and exposed to a heating cycle that is set to reach a temperature of 50 °C after 120 s of radio wave exposure.

There is a degree of variability between the power and temperature transients of these samples (Figure 10). The top right and bottom left graphs for 17.5 and 25 m%, respectively, show similar trends. In both graphs the recorded temperature follows an s-curve that approximates 50 °C, while the curve of net radio wave power transfer has a triangular shape. The graph for the 10 m% sample (top left) has a similar s-shaped curve for temperature, but the net power transfer curve deviates somewhat from a triangular shape. The graph for the loosely packed 25 m% humidity sample (bottom right) exhibits strong oscillations in the power curve. It appears that the loose packing increases the delay between power input and temperature effect to a greater degree than what the predictive control system anticipates, this results in repeated overcorrections and oscillations. This suggests that consistent sample preparation is essential.

The second experimental demonstration is a series of tests with soil samples that were obtained from horticulture growers and are inoculated with nematodes of species *S. feltiae*. These samples are each exposed to a radio wave field of various

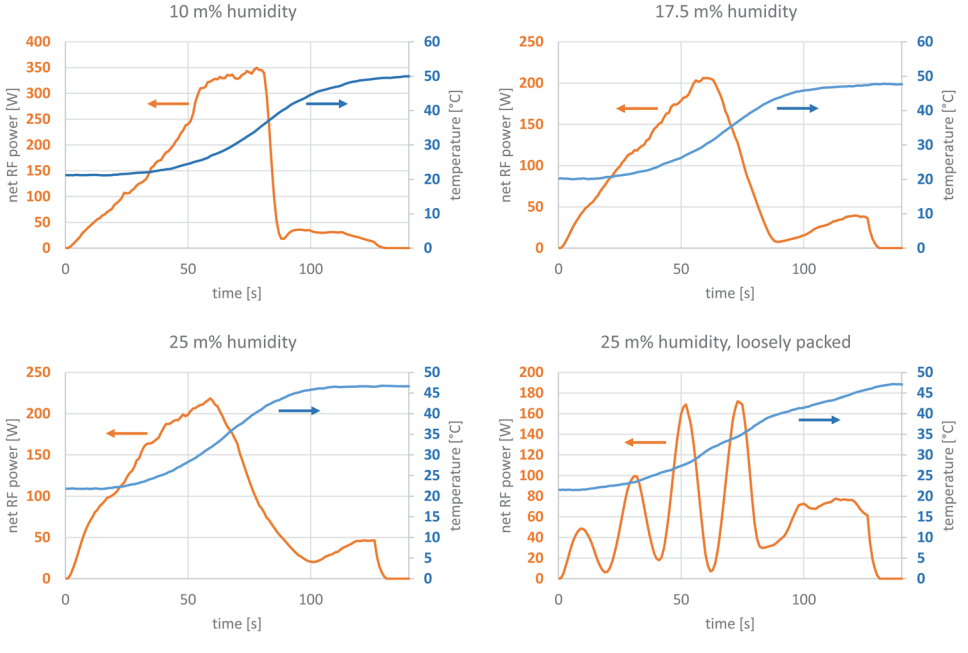

Figure 10. Transients of the net radio wave power transmission and sample temperature for four different cases of heating a sample in the Tweik-apparatus. Soil of three different humidities is used, in one case the soil is only loosely packed in the sample holder.

intensity. Samples are prepared by first drying soil overnight at 105 °C. Subsequently, at room temperature, water and nematodes are introduced into the sample. Nematodes dissolved in water are added to the sample by making a hole in the soil column with a finger, pipetting a measured amount of the nematode solution, and gently closing the hole again with a nominal number of 1000 nematodes each.

During the series of experiments, the samples are heated from room temperature of around 20 °C to a pre-determined setpoint temperature. The setpoint values are varied between 40 °C and 60 °C over the set of samples. After radio wave heating, the samples are left to cool to room temperature in their sample holder outside of the cavity in air. Cooldown takes around an hour. Once room temperature is reached, the samples are repackaged for further analysis.

The effectiveness of radio wave treatment is assessed by counting the number of live nematodes remaining in the samples by means of an Oostenbrink elutriator as described by Verschoor and de Goede (2000). The soil sample is added to the elutriator, which separates the heavy soil particles from the lighter nematodes using an upflow of water. The water containing the nematodes is subsequently drained through and incubated on a filter for 24 h, after which the nematodes that remained alive have migrated through this filter. They are harvested from a receptacle with water, and subsamples are counted.

Table 1 presents the results of this series of experiments. The samples are heated to setpoint temperatures of 40, 45, 50, 55, or 60 °C, with three repeated experiments per temperature. The table includes the mass of the individual samples, which varies between 130 and 140 g. In addition, the table reports the recorded maximum temperature and the specific radio wave exposure, i.e. the amount of radio wave energy that is dissipated into heat per unit sample mass. Finally, the table also includes two resulting nematode counts per sample. For one sample, nr. 14, unfortunately it appears a mishap occurred since no nematodes could be found. For the remaining samples the results are graphed (Figure 11). The results are presented both as nematode count versus maximum recorded temperature as well as count versus the amount of radio wave energy dissipated in the sample per unit sample mass.

Table 1. Sample specifications and experimental data.

Sample number	Sample mass	Temperature setpoint	Maximum temperature	Net specific radio wave exposure	Nematode count #1	Nematode count #2
	g	°C	°C	J/g	nr.	nr.
1	132.4	60	58.9	89.0	28	29
2	134.1		61.5	85.7	85	86
3	138.5		60.7	85.2	23	27
4	143.4	55	59.4	83.2	29	31
5	133.4		54.8	73.3	100	93
6	136.3		57.4	83.0	51	49
7	136.0	50	50.1	57.9	265	314
8	136.8		50.4	60.5	244	267
9	138.7		50.5	57.8	79	90
10	138.5	45	47.3	52.8	184	167
11	134.8		45.1	50.7	181	199
12	136.1		45.8	46.4	449	459
13	132.2	40	39.8	37.4	514	535
14	134.1		39.8	34.9	–	–
15	133.8		40.0	36.1	281	298

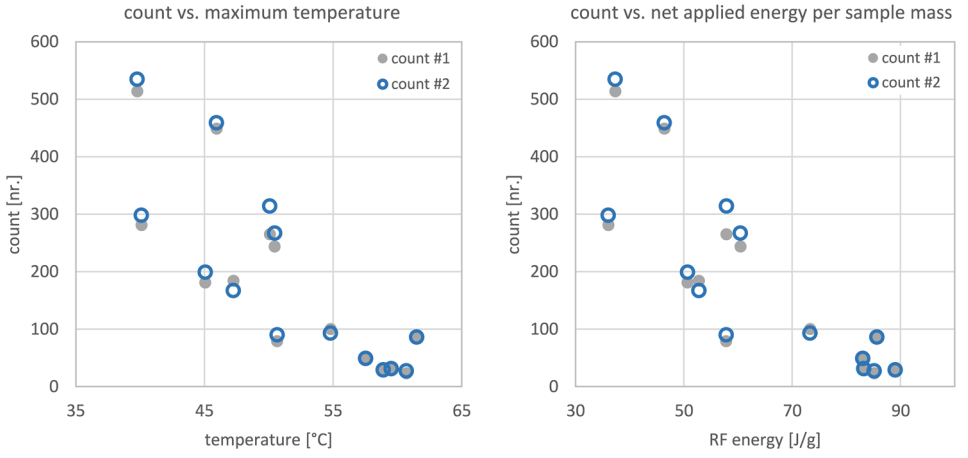

Figure 11. Nematode count versus radio wave intensity. The left graph presents the intensity in terms of maximum recorded temperature, while the right one presents it as the amount of radio wave energy dissipated in the sample per unit sample mass.

Both graphs have the same general trend: as the intensity of the radio wave exposure increases, less live nematodes remain. There are some minor changes in shape between the clouds of data points in the graphs, most likely because of slight differences in the distribution of heat generation and temperature between the sample, but overall the two graphs are consistent with each other. There are deviations in the maximum recorded temperature with respect to the temperature set-point. These fluctuations are likely due to variations between the respective samples, though this does not affect the overall trend. There does seem to be a large variation in nematode count at lower intensity, however. At this stage, it is not clear what may have caused this, but variations in sample mixing are suspected. Further refinement of the experimental protocol would be a fitting topic for further development.

Conclusions

This study describes the development of an experimental method that mimics the conditions in soil that is being treated by radio wave energy to suppress pathogens. It enables experimentation at laboratory scale with soil samples of 100 ml volume under much more controlled and reproducible conditions than can be achieved under field conditions with the Agritron prototype. Moreover, laboratory scale experimentation is considerably more cost-effective than field trials, so it facilitates a data driven approach towards developing treatment strategies for radio wave treatment of soil in glasshouse horticulture.

This paper documents the design requirements, implementation and operation of the apparatus that implements the experimental method. It heats soil samples uniformly with a triangular temporal power profile to a pre-determined temperature over the course of two minutes, which resembles soil treatment by the Agritron prototype.

The system design is based on a standard sized rectangular waveguide; special holders are designed to contain the soil samples; a tuning recommendation is

developed through numerical simulation; and a model-based predictive control strategy is employed to achieve heating according to the desired power profile to the desired final temperature. The method is demonstrated by a series of experiments. Plausible relations between radio wave exposure and pathogen effects are observed.

Acknowledgments

This research was performed in the framework of Kas als Energiebron, the Dutch innovation and action programme, for saving energy and applying sustainable energy in greenhouse horticulture, of Glastuinbouw Nederland and the Dutch Ministry of Agriculture, Nature and Food Quality. Contract number 1400 0103 54, reference number DGA-PAV/1917 8589. Our thanks go out to Tuinbouwbedrijf A. Baatje b.v. and MC GRAND b.v. for providing soil samples, and for facilitating field trials. Our thanks go out to Vacutech B.V., Verborg Engineering B.V., PIA Automation B.V. and Giel Hermans of the Electronic and Mechanical Support Division of TU Delft for their swift technical support. Special thanks go out to Bart Hoek of the Process & Energy department of TU Delft for his continued and prompt technical support.

Disclosure statement

No potential conflict of interest was reported by the author(s).

Notes on contributor

The research was performed as part of a collaborative project between Koppert Machines (KM), Stichting Control in Food & Flowers (SCFF), Groen Agro Control (GAC), and Delft University of Technology (DUT). The roles in relation to this present study are: G. Sturm (DUT), experimental design specification, sample holder and control system design, system integration, writing; J. Bonnet (SCFF) and A. v.d. Wurff (GAC), biological tests; A. Koppert and S. Linnenbank (KM), microwave circuit design and production.

ORCID

G. S. J. Sturm http://orcid.org/0000-0003-0035-0572
S. Linnenbank http://orcid.org/0000-0002-7796-9667
A. van der Wurff http://orcid.org/0000-0001-9040-4209

Data availability statement

Data will be made available on request.

References

Abbey L, Udenigwe C, Mohan A, Anom E. 2017. Microwave irradiation effects on vermicasts potency, and plant growth and antioxidant activity in seedlings of Chinese cabbage (Brassica rapa subsp. pekinensis). J Radiat Res Appl Sci. 10(2):110–116. doi: 10.1016/j.jrras.2017.01.002.

Agro Energy. 2017. *De elektriciteitsmarkt in vogelvlucht in de tuinbouw*. [Online] [Accessed 2020 Mar 9]. https://www.agro-energy.nl/wp-content/uploads/2017/03/Whitepaper_Energiemarkt_in_vogelvlucht_LR.pdf.

Aguilar Garib J. 2022. Editor's message: the solid-state applications era. J Microw Power Electromagn Energy. 56(1):1–2. doi: 10.1080/08327823.2022.2033454.
Anton Paar GmbH. 2021. *Microwave reactor: monowave*. [Online]. [Accessed 2021 Dec 15]. https://www.anton-paar.com/corp-en/products/details/microwave-synthesis-monowave-400200/
Barker K, Gooding G, Elder A, Eplee R. 1972. Killing and preserving nematodes in soil with chemicals and microwave energy. J Nematol. 4(2):75–79.
Bollen G. 1969. The selective effect of heat treatment on the microflora of a greenhouse soil. Netherlands J Plant Pathol. 75(1–2):157–163. doi: 10.1007/BF02137211.
Boom TJJ van den, de Vries RAJ. 1999. Robust predictive control using a time-varying Youla parameter. Int J Appl Math Comput Sci. 9(1):101–128. [Accessed 2023 Jan 4] https://www.amcs.uz.zgora.pl/?action=download&pdf=AMCS_1999_9_1_4.pdf
Brodie G, et al. 2015. Assessing the impact of microwave treatment on soil microbial populations. Global J Agric Innov Res Develop. 2(1):25–32. doi: 10.15377/2409-9813.2015.02.01.3.
Brodie G, Khan M, Gupta D. 2020a. Microwave soil treatment and plant growth. In M. Hasanuzzaman, M. Fujita, M. Teixeira Filho & T. Nogueira, editors. Sustainable crop production. London: TechOpen. doi: 10.5772/intechopen.89684.
Brodie G, Pchelnikov Y, Torgovnikov G. 2020b. Development of microwave slow-wave comb applicators for soil treatment at frequencies 2.45 and 0.922 GHz (theory, design, and experimental study). Agriculture. 10(12):604. doi: 10.3390/agriculture10120604.
Brodie G, Ryan C, Lancaster C. 2012. Microwave technologies as part of an integrated weed management strategy: a review. Int J Agron. 2012:1–14. doi: 10.1155/2012/636905.
Brown E. 2022. The next-generation consumer microwave oven: a review. J Microw Power Electromagn Energy. 56(2):82–86. doi: 10.1080/08327823.2022.2066772.
Camacho E, Bordons C. 1995. Model predictive control in the process industry. London: Springer-Verlag.
CEM Corporation. 2020. *Discover microwave synthesizer*. [Online] [Accessed 2021 Dec 15]. https://cem.com/en/discover.
Chen Y, Gamliel A, Stapleton J, Aviad T. 1991. Chemical, physical, and microbial changes related to plant growth in disinfested soil. In: J. Katan and J. DeVay, editors. Soil solarization. Boca Raton: CRC Press.
Clarke D, Mohtadi C, Tuffs P. 1987. Generalized predictive control—part I. The basic algorithm. Automatica. 23(2):137–148. doi: 10.1016/0005-1098(87)90087-2.
Comsol AB. 2019. COMSOL multiphysics 5.5. Stockholm: S.N.
Conchado A, Linares P 2012. The economic impact of demand-response programs on power systems. a survey of the state of the art. In: A. Sorokin, et al. editors. Handbook of networks in power systems I. Energy systems. Berlin: Heidelberg.
Cutler C, Ramaker B. 1980. Dynamic matrix control—a computer control algorithm. Proceedings of the Joint Automatic Control Conference, San Francisco.
Dabbene F, Gay P, Tortia C. 2003. Modelling and control of steam soil disinfestation processes. Biosyst Eng. 84(3):247–256. doi: 10.1016/S1537-5110(02)00276-3.
Eglitis M, Johnson F. 1970. Control of seedling damping-off in greenhouse soils by radio frequency energy. Plant Disease Reporter. 54(3):268–271.
Eglitis M, Johnson F, Breakey E. 1956. Soil pasteurization with high frequency energy (abstract). Phytopathology. 46(11):635–636.
European and Mediterranean Plant Protection Organization (OEPP/EPPO). 2013. PM 7/119 (1) Nematode extraction. Bull OEPP/EPPO Bull. 43(3):471–495. doi: 10.1111/epp.12077.
Ferriss R. 1984. Effects of microwave oven treatment on microorganisms in soil. Phytopathology. 74(1):121–126. doi: 10.1094/Phyto-74-121.
Franklin G, Powell J, Emami-Naeini A. 1994. Feedback control of dynamic systems. 3rd ed. Reading MA: Addison-Wesley.
Fujikawa H, Itoh T. 1998. Thermal inactivation analysis of mesophiles using the Arrhenius and z-value models. J Food Prot. 61(7):910–912. doi: 10.4315/0362-028X-61.7.910.
Griffin G, Baker R. 1991. Population dynamics of plant pathogens and associated organisms in soil in relation to infectious inoculum. In J. Katan and J. DeVay, editors. Soil solarization. Boca Raton: CRC Press.

Hess M, Buisson E, Mesléard F. 2019. Soil compaction enhances the impact of microwave heating on seedling emergence. Flora. 259:151457. doi: 10.1016/j.flora.2019.151457.
Hess MCM, De Wilde M, Yavercovski N, Willm L, Mesléard F, Buisson E. 2018. Microwave soil heating reduces seedling emergence of a wide range of species including invasives. Restor Ecol. 26(S2):S160–S169. doi: 10.1111/rec.12668.
International Telecommunication Union. 2020. *Radio regulations*. [Online] [Accessed 2022 Sept 19]. https://www.itu.int/dms_pub/itu-r/opb/reg/R-REG-RR-2020-ZPF-E.zip
Kappe C. 2013. How to measure reaction temperature in microwave-heated transformations. Chem Soc Rev. 42(12):4977–4990. doi: 10.1039/c3cs00010a.
Katan, J, DeVay, J. editors. 1991a. Soil solarization. Boca Raton: CRC Press.
Katan J, DeVay J. 1991b. Soil solarization: historical perspectives, principles, and uses. In: J. Katan and J. DeVay, editors. Soil solarization. Boca Raton: CRC Press.
Khan MJ, Brodie G, Gupta D. 2016. Effect of microwave (2.45 GHz) treatment of soil on yield components of wheat (Triticum aestivum L.). J Microw Power Electromagn Energy. 50(3):191–200. doi: 10.1080/08327823.2016.1228441.
Koppert Machines. 2014. *20140327 koppertmachines agritron*. [Online] [Accessed 2020 Jan 24]. https://www.youtube.com/watch?v=Rdk4JZnOKig.
Ljung L. 1999. System identifiation—theory for the user. 2nd ed. Upper Saddle River NJ: Prebtice Hall.
Mahdi W, Al-Badri K, Alqaisi M. 2021. Effect of microwave radiation on bacteria, fungi and some growth characteristics of cowpea Vigna unguiculata L. Gesunde Pflanzen. 73 (2):161–167. doi: 10.1007/s10343-020-00534-2.
Maynaud G, Baudoin E, Bourillon J, Duponnois R, Cleyet-Marel J-C, Brunel B. 2019. Short-term effect of 915-MHz microwave treatments on soil physicochemical and biological properties. European J Soil Sci. 70(3):443–453. doi: 10.1111/ejss.12769.
Menges R, Wayland J. 1974. UHF electromagnetic energy for weed control in vegetables. Weed Sci. 22(6):584–590. doi: 10.1017/S0043174500038352.
Meredith R. 1998. Engineers' handbook of industrial microwave heating. London: Institution of Electrical Engineers.
Miler N, Kulus D. 2018. Microwave treatment can induce chrysanthemum phenotypic and genetic changes. Sci Hortic. 227(227):223–233. doi: 10.1016/j.scienta.2017.09.047.
Milestone Srl. 2021. [Accessed 2021 Dec 15]. https://www.milestonesrl.com/products/microwave-digestion/ethos-up.
Mills A. 1999. Basic heat & mass transfer. 2nd ed. New Jersey: Prentice-Hall.
Nelson S. 1996. A review and assessment of microwave energy for soil treatment to control pests. Transac ASAE. 39(1):281–289. doi: 10.13031/2013.27508.
Nelson S, Stetson L. 1974. Comparative effectiveness of 39- and 24S0-MHz electric fields for control of rice weevils in wheat. J Econ Entomol. 67(5):592–595. doi: 10.1093/jee/67.5.592.
Nickel H-U. 2022. *TD-00036 – Cross reference for hollow metallic waveguide*. [Accessed 2024 Feb 22]. https://www.microwaves101.com/uploads/TD-00036S-Ulis-waveguide-list.pdf.
O'Bannon J, Good J. 1971. Application of microwave energy to control nematodes in soil. J Nematol. 3(1):93–94.
Ogata K. 2002. Modern control engineering. 4th ed. New Jersey: Prentice-Hall.
Peleg M, Normand M, Corradini M. 2012. The Arrhenius equation revisited. Crit Rev Food Sci Nutr. 52(9):830–851. doi: 10.1080/10408398.2012.667460.
Pozar D. 2005. Microwave engineering. 3rd ed. Hoboken: Wiley.
Pullman G, DeVay J, Garber R. 1981. Soil solarization and thermal death—a logarithmic relationship between time and temperature for four soilborne pathogens. Phytopathology. 71(9):954–959. doi: 10.4315/0362-028X-61.7.910.
Rasing F, Jansen W. 2007. *Diëlektrisch ontsmetten van substraten - Een goed alternatief voor stromen?*. [Accessed 2020 Mar 9]. https://edepot.wur.nl/117179.
Richalet J, Rault A, Testud J, Papon J. 1978. Model predictive heuristic control: applications to industrial processes. Automatica. 14(5):413–428. doi: 10.1016/0005-1098(78)90001-8.

Roux-Michollet D, Dudal Y, Jocteur-Monrozier L, Czarnes S. 2010. Steam treatment of surface soil: how does it affect water-soluble organic matter, C mineralization, and bacterial community composition? Biol Fertil Soils. 46(6):607–616. doi: 10.1007/s00374-010-0468-6.

Seaman W, Wallen V. 1967. Effect of exposure to radio-frequency electric fields on seed-borne microorganisms. Can J Plant Sci. 47(1):39–49. doi: 10.4141/cjps67-006.

Soeterboek A. 1990. Predictive control—a unified approach [PhD thesis]. Delft: Delft University of Technology.

Sturm GSJ, Stefanidis GD, Verweij MD, Van Gerven TDT, Stankiewicz AI. 2010. Design principles of microwave applicators for small-scale process equipment. Chem Eng Process. 49(9):912–922. doi: 10.1016/j.cep.2010.07.017.

Sturm GSJ, Van Braam Houckgeest AQ, Verweij MD, Van Gerven T, Stankiewicz AI, Stefanidis GD. 2013b. Exploration of rectangular waveguides as a basis for microwave enhanced continuous flow chemistries. Chem Eng Sci. 89:196–205. doi: 10.1016/j.ces.2012.11.039.

Sturm GSJ, Verweij MD, van Gerven T, Stankiewicz AI, Stefanidis GD. 2012. On the effect of resonant microwave fields on temperature distribution in time and space. Int J Heat Mass Transf. 55(13–14):3800–3811. doi: 10.1016/j.ijheatmasstransfer.2012.02.065.

Sturm GSJ, Verweij MD, Gerven T v, Stankiewicz AI, Stefanidis GD. 2013a. On the parametric sensitivity of heat generation by resonant microwave fields in process fluids. Int J Heat Mass Transf. 57(1):375–388. doi: 10.1016/j.ijheatmasstransfer.2012.09.037.

Sturm GSJ, van der Wurff A, Linnenbank S, Bonnet J, Koppert A. 2023. Numerical simulation framework for radio wave soil treatment for pathogen suppression. Comput Electron Agric. 211:107992. doi: 10.1016/j.compag.2023.107992.

Sturm GSJ, van der Wurff A, Linnenbank S, Bonnet J, Koppert A. 2024. Numerical parametric study of radio wave soil treatment for pathogen suppression. Comput Electron Agric. 222:108998. doi: 10.1016/j.compag.2024.108998.

The Mathworks. 2019. MATLAB R2019b. Natrick: SN.

Tkalec M, Malarić K, Pavlica M, Pevalek-Kozlina B, Vidaković-Cifrek Z. 2009. Effects of radiofrequency electromagnetic fields on seed germination and root meristematic cells of Allium cepa L. Mutat Res. 672(2):76–81. doi: 10.1016/j.mrgentox.2008.09.022.

Verschoor B, de Goede R. 2000. The nematode extraction efficiency of the Oostenbrink elutriator-cottonwool filter method with special reference to nematode body size and life strategy. Nematol. 2(3):325–342. doi: 10.1163/156854100509204.

Wayland J, Merkle M, Davis F, Menges RM, Robinson R. 1975. Control of weeds with UHF electromagnetic fields. Weed Res. 15(1):1–5. doi: 10.1111/j.1365-3180.1975.tb01088.x.

Welle A. v. d. 2016. *Ontwerp van elektriciteitsmarkten – benodigde aanpassingen voor een flexibeler energiesysteem op korte termijn*. [Accessed 2020 Mar 9]. https://repository.tno.nl/islandora/object/uuid%3A2df73fc0-25bf-4a83-a170-1349a66bef9d.

Werner K. 2020. The impact of solid-state RF technology on product development. In U. Erle, P. Pesheck and M. Lorence, editors. Development of packaging and products for use in microwave ovens. 2nd ed. Duxford: Woodhead Publishing, p. 415–431. doi: 10.1016/B978-0-08-102713-4.00015-3.

Appendix A

At each time step, a predictive controller acquires sensor data from the process that it is controlling, and it uses this data to optimize the input signals to this plant so that the output signals follow a desired trajectory. This appendix describes the predictive controller that controls temperature in soil samples that are heated the Tweik-apparatus. It is a single input/single output control system. In addition, it is also necessarily a digital control system, as required for repeated numerical optimization. The input (**u**) and output (**y**) signals are represented by vectors of input and output variable values over a finite time horizon with length L,

$$\mathbf{u}=\begin{bmatrix} u_1 \\ u_2 \\ \vdots \\ u_L \end{bmatrix}=\begin{bmatrix} u(t=0) \\ u(t=h) \\ \vdots \\ u(t=h(L-1)) \end{bmatrix},\quad \mathbf{y}=\begin{bmatrix} y_1 \\ y_2 \\ \vdots \\ y_L \end{bmatrix}=\begin{bmatrix} y(t=0) \\ y(t=h) \\ \vdots \\ y(t=h(L-1)) \end{bmatrix} \tag{5}$$

The basis of a predictive controller is a model description of the process that it uses for the optimization. The model description is a linear model, either of the finite impulse response (FIR) or finite step response (FSR) type. Predicting the response of a linear model to an input signal is done by calculating the convolution integral of this input signal with the impulse response of the model. For discrete-time systems, this can be conveniently represented as a matrix vector multiplication,

$$\boldsymbol{\delta}\mathbf{u}=\mathbf{y} \tag{6}$$

Here, the column vectors of the matrix $\boldsymbol{\delta}$ each contains the impulse response sequence. The impulse response vectors in the matrix are progressively shifted downward with each consecutive column, with zero padding in front of the response to fill the vector. This representation is a FIR model. However, for the control system in this present study, FSR model is more appropriate, because it has a better steady state and low frequency response. Specifically, if a steady state or low frequency mismatch between the process and the model of the process were to occur, which is practically unavoidable in the present case, then an FSR model description can accommodate this, while the FIR description cannot. For an FSR model, the model output is calculated by convolution of the step response with the time derivative of the input signal. This is represented herein as multiplication of a matrix with step responses **S** in the column vectors with a vector of incremental variations $\Delta\mathbf{u}$ of the input signal,

$$\mathbf{S}\Delta\mathbf{u}=\mathbf{y},\ u_{l+1}=u_l+\Delta u_l \tag{7}$$

which is represented in more detail as,

$$\begin{bmatrix} 0 & 0 & \cdots & 0 \\ S_1 & 0 & & 0 \\ S_2 & S_1 & & \vdots \\ \vdots & & \ddots & 0 \\ S_{L-1} & S_{L-2} & \cdots & S_1 \end{bmatrix}\begin{bmatrix} \Delta u_1 \\ \Delta u_2 \\ \vdots \\ \Delta u_{L-1} \end{bmatrix}=\begin{bmatrix} y_1 \\ y_2 \\ \vdots \\ y_L \end{bmatrix} \tag{8}$$

The model representation in Eq. (8) over L time steps is split over the past and future events, of N and M time steps respectively, where, $L = N + M$. This results in,

$$\begin{bmatrix} \begin{bmatrix} 0 & 0 & \cdots & 0 \\ S_1 & 0 & & \\ S_2 & S_1 & \ddots & \vdots \\ \vdots & \vdots & & \\ S_{N-1} & S_{N-2} & \cdots & 0 \end{bmatrix} & \begin{bmatrix} 0 & \cdots & \cdots & 0 \\ & & & \\ \vdots & & & \vdots \\ & & & \\ 0 & \cdots & \cdots & 0 \end{bmatrix} \\ \begin{bmatrix} S_N & S_{N-1} & \cdots & S_1 \\ S_{N+1} & S_N & & \\ S_{N+2} & S_{N+1} & & \vdots \\ \vdots & \vdots & \ddots & \\ S_{M+N-1} & S_{M+N-2} & \cdots & S_M \end{bmatrix} & \begin{bmatrix} 0 & 0 & \cdots & 0 \\ S_1 & 0 & & \\ S_2 & S_1 & & \vdots \\ \vdots & \vdots & \ddots & 0 \\ S_{M-1} & S_{M-2} & \cdots & S_1 \end{bmatrix} \end{bmatrix} \begin{bmatrix} \begin{bmatrix} \Delta u_{p,1} \\ \vdots \\ \Delta u_{p,N} \end{bmatrix} \\ \begin{bmatrix} \Delta u_{f,1} \\ \vdots \\ \Delta u_{f,M-1} \end{bmatrix} \end{bmatrix} = \begin{bmatrix} \begin{bmatrix} y_{p,1} \\ \vdots \\ y_{p,N} \end{bmatrix} \\ \begin{bmatrix} y_{f,1} \\ \vdots \\ y_{f,M} \end{bmatrix} \end{bmatrix} \tag{9}$$

Writing it in more compact form with some adjustments yields,

$$-y_0 + \begin{bmatrix} \mathbf{S}_{pp} & 0 \\ \mathbf{S}_{fp} & \mathbf{S}_{ff} \end{bmatrix} \begin{bmatrix} \Delta \mathbf{u}_p + \mathbf{e}_{i,p} \\ \Delta \mathbf{u}_f + \mathbf{e}_{i,f} \end{bmatrix} = \begin{bmatrix} \mathbf{m}_p + \mathbf{e}_{o,p} \\ \mathbf{r}_f + \mathbf{e}_{o,f} \end{bmatrix} - m_{p,N} \tag{10}$$

The signals $\mathbf{m}_p$ and $\mathbf{r}_f$ represent respectively, the past measurements of the controlled variable temperature, and the future reference trajectory of the controlled variable. Here the final time step of the past events is made to approximate zero, so that the signal optimization is performed around zero. To this end, the left side of Eq. (10) includes a subtraction of,

$$y_0 = \begin{bmatrix} S_{N-1} & \cdots & S_1 & 0 \end{bmatrix} \begin{bmatrix} \Delta u_{p,1} \\ \vdots \\ \Delta u_{p,N} \end{bmatrix} \tag{11}$$

and the right side includes a subtraction of the most resent measurement of temperature,

$$m_{p,N} \approx y_{p,N} \tag{12}$$

Moreover, Eq. (10) introduces error signals that represent the mismatch between signals that occur in the model and signals that occur in the physical system. These error signals comprise of: $\mathbf{e}_{i,p}$, the error signal that acts on past input signals; $\mathbf{e}_{o,p}$ the error signal that acts on past output signals; $\mathbf{e}_{i,f}$ the error signal that acts on future input signals; and $\mathbf{e}_{o,f}$ the error signal that acts on future output signals. The two former of these account for the mismatch between the measured input and output signals, and those that occur in the controller model. Minimizing this mismatch enables the controller to estimate the state of the process that it is controlling. The two latter signals that relate to the future are used by the controller to calculate future input signals that minimize the difference between the future

process output signals and the desired future process output signals, i.e. the reference signal $\mathbf{r}_f$.

The control optimization is now solved in two steps. First the error signals of the past events are calculated by solving the top sub-matrices of Eq. (10),

$$-y_0 + \mathbf{S}_{pp}\left(\Delta\mathbf{u}_p + \mathbf{e}_{i,p}\right) = \mathbf{m}_p + \mathbf{e}_{o,p} - m_{p,N} \tag{13}$$

while subject to a cost function,

$$\min_{\left\{\mathbf{e}_{i,p}\,\mathbf{e}_{o,p}\right\}\in\mathbb{R}} \begin{bmatrix}\mathbf{e}_{i,p} & \mathbf{e}_{o,p}\end{bmatrix}\mathbf{Q}_p \begin{bmatrix}\mathbf{e}_{i,p}\\ \mathbf{e}_{o,p}\end{bmatrix} \tag{14}$$

This problem is solved as a quadratic program, which is a particular mathematical problem description that can be solved efficiently. This calculation involves an optimization that minimizes the error signals. The $\mathbf{Q}_p$ matrix can be designed to adjust the sensitivity between input and output error depending on the particular control problem.

Once the error signals of the past events are estimated, then in the second step the optimum trajectory of future control inputs is calculated that makes the system output follow the desired reference trajectory that is represented by the vector $\mathbf{r}_f$. To this end, the bottom row of sub-matrices of Eq. (10) is solved,

$$-y_0 + \mathbf{S}_{fp}\left(\Delta\mathbf{u}_p + \mathbf{e}_{i,p}\right) + \mathbf{S}_{ff}\Delta\mathbf{u}_f = \mathbf{r}_f + \mathbf{e}_{o,f} - m_{p,N} \tag{15}$$

assuming $\mathbf{e}_{i,f} = 0$ while subject to cost function,

$$\min_{\left\{\Delta\mathbf{u}_f\,\mathbf{e}_{o,f}\right\}\in\mathbb{R}} \begin{bmatrix}\Delta\mathbf{u}_f & \mathbf{e}_{o,f}\end{bmatrix}\mathbf{Q}_f \begin{bmatrix}\Delta\mathbf{u}_f\\ \mathbf{e}_{o,p}\end{bmatrix} \tag{16}$$

and the inequality constraints for the input power, i.e. $u(t) \geq 0$,

$$\begin{bmatrix}1\\ \vdots\\ 1\end{bmatrix}\left(u_{p,N} + \Delta u_{p,N}\right) + \begin{bmatrix}0 & 0 & \cdots & 0\\ 1 & 0 & & \vdots\\ 1 & 1 & & \vdots\\ \vdots & \vdots & \ddots & 0\\ 1 & 1 & \cdots & 1\end{bmatrix}\Delta\mathbf{u}_f \geq 0 \tag{17}$$

This problem too is a quadratic program and is solved as such.

The performance of the controller is tuned by designing $\mathbf{Q}_f$ so that the respective weights on $\Delta\mathbf{u}_f$ and $\mathbf{e}_{o,f}$ are adjusted so that their respective actions are brought to a desired balance between them. For example, putting more weight on minimizing the contribution of $\Delta\mathbf{u}_f$ to

the cost function will cause the output of the controlled process to follow the desired trajectory in a more relaxed fashion. In addition, the input signals as generated by the controller will have less sharp transient behavior. Furthermore, if the controlled system has a time delay, then an initial period can be defined in which $\mathbf{e}_{o,f}$ has no contribution to the cost function. This will make the controller tolerate a mismatch between the output signal and the desired reference signal during this period in which the controller has little or no control authority. This avoids sharp controller action in an attempt to control temperature in the nearest future time steps, which in the case of our experimental method results in a smoother radio wave power transient.